RESEARCH ARTICLE | SEPTEMBER 22 2022

Fabrication of microstructures on curved hydrogel substrates

Special Collection: Papers from the 65th International Conference on Electron, Ion, And Photon Beam Technology and Nanofabrication (EIPBN 2022)

M. Chen; X. Ding; L. Que; ... et. al

Journal of Vacuum Science & Technology B 40, 052804 (2022)
https://doi.org/10.1116/6.0002071

JVST B
Journal of Vacuum Science & Technology B

ARTICLE

avs.scitation.org/journal/jvb

Fabrication of microstructures on curved hydrogel substrates

Cite as: J. Vac. Sci. Technol. B 40, 052804 (2022); doi: 10.1116/6.0002071
Submitted: 8 July 2022 · Accepted: 19 August 2022 ·
Published Online: 22 September 2022

M. Chen,[1] X. Ding,[2] L. Que,[2,a)] and X. Liang[1,b)]

AFFILIATIONS

[1]Mechanical Engineering Department, University of Michigan, Ann Arbor, Michigan 48109
[2]Department of Electrical and Computer Engineering, Iowa State University, Ams, Iowa 50011

Note: This paper is part of the Special Topic Collection: Papers from the 65th International Conference on Electron, Ion, And Photon Beam Technology and Nanofabrication (EIPBN 2022).

[a)]**Electronic mail:** lque@iastate.edu
[b)]**Electronic mail:** xiaoganl@umich.edu

ABSTRACT

Emerging wearable devices are very attractive and promising in biomedical and healthcare fields because of their biocompatibility for monitoring *in situ* biomarker-associated signals and external stimulus. Many such devices or systems demand microscale sensors fabricated on curved and flexible hydrogel substrates. However, fabrication of microstructures on such substrates is still challenging because the traditional planar lithography process is not compatible with curved, flexible, and hydrated substrates. Here, we present a shadow-mask-assisted deposition process capable of directly generating metallic microstructures on the curved hydrogel substrate, specifically the contact lens, one of the most popular hydrogel substrates for wearable biomedical applications. In this process, the curved hydrogel substrate is temporarily flattened on a planar surface and metal features are deposited on this substrate through a shadow mask. To achieve a high patterning fidelity, we have experimentally and theoretically investigated various types of distortion due to wrinkles on 3D-printed sample holders, geometric distortion of the substrate due to the flattening process, and volume change of the hydrogel material during the dehydration and hydration processes of the contact lens. Using this method, we have demonstrated fabrication of various titanium pattern arrays on contact lenses with high fidelity and yield.

I. INTRODUCTION

Wearable devices have drawn enormous interest because of their capability of continuously and instantaneously measuring various biological signals and stimulus, such as glucose level, heart rate, and light field, without causing any discomfort.[1–4] Among all the wearable device substrates, hydrogel substrates, such as contact lenses and artificial skins, have attracted huge attention because of their superior biocompatibility and mechanical properties.[5–7] However, to generate functional metallic microstructures on such flexible hydrogel substrates, the metal layers need to be robust enough and have good adhesion to the substrates to endure the potential deformation of hydrogel in real applications. Current smart contact lenses with embedded metal structures are fabricated by sandwiching metal patterns on the sacrificial layer inside the contact lenses and curing them together.[8,9] Such integrated metal microstructures inside curved and flexible hydrogel substrates induce unwanted mechanical stress that could break the contact lenses and irritate users' eyes. In addition, such a fabrication process cannot meet the requirements for functionalizing commercially viable contact lenses with customized functions, therefore limiting their application scope.

In this article, we present a shadow-mask-assisted flattening and deposition (SFD) method, which combines a silicon shadow mask with predefined patterns and a regular physical vapor deposition method, capable of generating arbitrary metallic patterns on curved and flexible hydrogel substrates. Using this method, we have successfully fabricated square arrays and concentric rings of Ti on contact lenses and explored the decisive factors responsible for the distortion of the deposited metal pattern. Our research mainly discussed three types of pattern distortions of the hydrogel material caused in the fabrication process, including (i) wrinkles imprinted

by 3D-printed sample holders; (ii) geometric change of the curved sphere in the flattening process, and (iii) volumetric change of the hydrogel material during the transition between dehydrated and hydrated phases. Through comparing the dimensions of the deposited square arrays on the contact lenses dried on different sample holders, we find that the holder with a smoother surface leads to less distortion of the metallic patterns. In addition, the finite element simulation (FEA) results show that the flattening process generates a planar strain of 3%. Furthermore, by applying a constant mechanical load on the shadow mask during the dehydration course, the dehydration-induced volume change of the hydrogel material could be largely suppressed and minimized. Finally, a functional contact lens bearing concentric ring patterns is utilized to demonstrate the quantification of the intraocular pressures.

II. EXPERIMENTS

A. Sample preparation

Figures 1(a) and 1(b) display the schematic illustration and photo of our experimental setup for performing the SFD process, respectively. Specifically, a hydrated contact lens (Johnson & Johnson, Inc.) is placed on a 3D-printed sample holder. The lens is properly centered to the truncated-cone feature on the holder by aligning its edge with the bottom edge of the holding cone. The central region of the lens for metal deposition is conformally flattened on the holder through briefly pumping away the trapped air between the lens and the holder. Afterward, a silicon-based shadow-mask bearing predefined features is applied on top of the contact lens and aligned with the flattened region of the lens through aligning the holes on the shadow mask with the mounting pillars on the sample holder. After an overnight drying process, the dehydrated contact lens sandwiched by the shadow mask and the sample holder is loaded into an electron-beam evaporator (Enerjet Evaporator) and deposited with 30 nm thick Ti at a deposition rate of 1 Å/s. Here, Ti is chosen because of its good adhesion to the contact lens and hard-tissue compatibility.[10–13] After deposition, the contact lens with as-deposited Ti features is soaked into the standard contact lens solution for 5 min for rehydrating the contact lens. Finally, the Ti-based patterns (concentric rings or square arrays) are successfully produced on the curved and hydrated contact lens.

B. 3D-printing of the sample holder

A typical sample holder is printed by using a 3D printer (Form 3+, Formlabs) implementing the stereolithography (SLA) method, which results in a high printing resolution and smooth surface of the sample holder. The truncated-cone feature has a radius of 7.1 and 4.2 mm for bottom and top circles, respectively, and a height of 2.67 mm. The sample holder is designed to have conformal contact with the contact lens, especially the flattened

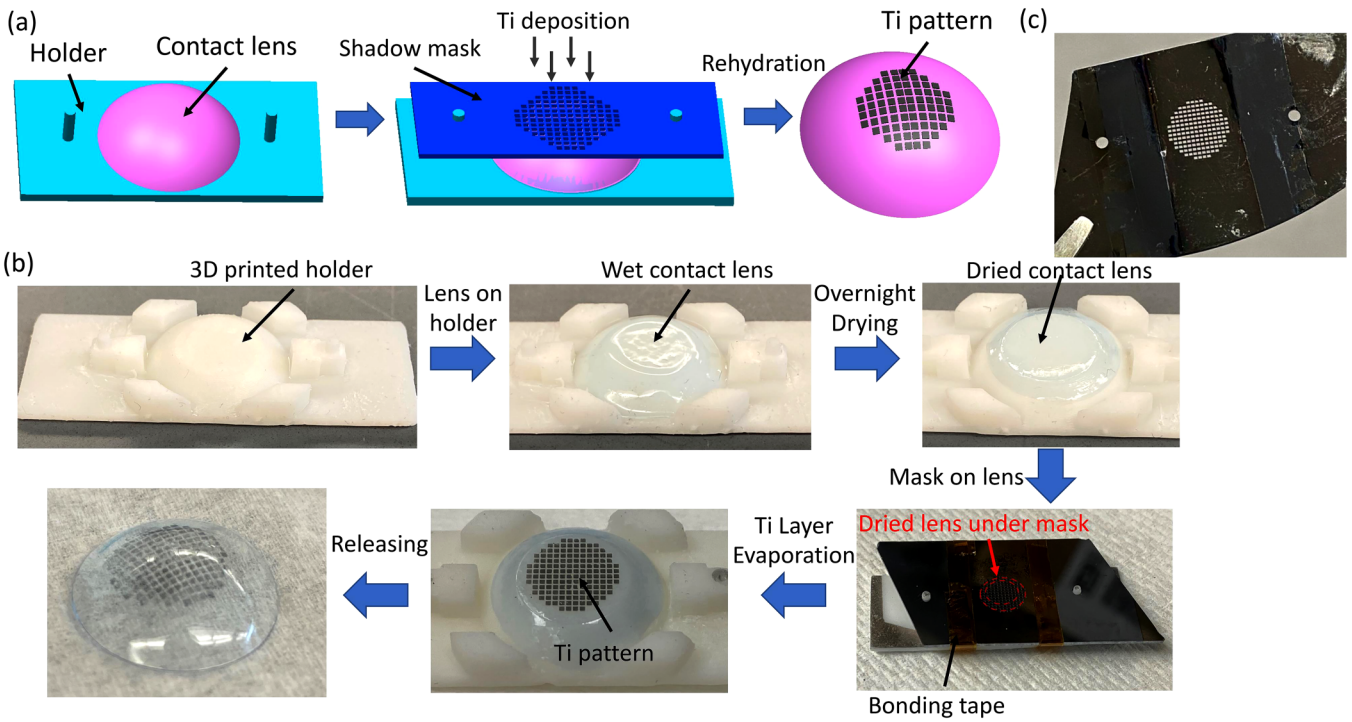

FIG. 1. Setup of the shadow-mask-assisted flattening and deposition (SFD) method: (a) schematic flow chart of the SFD method; (b) a set of photos displaying a SFD process for depositing metallic patterns on one type of the most popular hydrogel substrates, the contact lens; (c) photo of a representative shadow-mask bearing an array of squares of 400 μm length and 100 μm spacing.

central region of the lens to be deposited with metallic microstructures.

C. Fabrication of the shadow mask

A photoresist (SPR220) is spin-coated on a 500 μm thick Si template substrate using a CEE 200× spinner at 3000 rpm. After 115 °C baking for 90 s, the template substrate is aligned with the mask bearing square array patterns with 400 μm size and 500 μm period or concentric ring features with 100 μm width and 200 μm period, and exposed to UV light using an aligner (MJB3-2). After the developing process, the exposed patterns on the substrate are etched through using an STS Pegasus tool. Afterward, the substrate is cleaned by O2 plasma [YES-CV200RFS(E)] for 5 min and soaked into a nanostrip tool overnight to completely eliminate the residual photoresist on the fabricated shadow mask.

D. Intraocular pressure measurement

Using the process described in Sec. II A, a concentric ring grating has been fabricated on a contact lens, which is used as the intraocular pressure (IOP) sensor. As a technical demonstration, the contact lens IOP sensor is mounted on a silicone eye model to monitor the IOP.[14]

III. RESULT AND DISCUSSION

Figure 2(a) illustrates an as-deposited metallic pattern on a contact lens. In this fabrication work, we have identified three critical types of distortion that prominently affect the final pattern quality. First, the contact lens dried on the sample holder with a 3D-printing-formed rough surface exhibits wrinkles imprinted by such a rough surface, inducing the distortion illustrated in Fig. 2(b). Second, the central region of the lens needs to be flattened for metal deposition. After deposition, it is elastically recovered back to its original spherical cap shape. During this recovering process, the deposited metal features are expected to undergo a geometric transformation, as illustrated in Fig. 2(c). In addition, the huge volume change during the dehydration/hydration circle of the hydrogel material generates surface strain, leading to pattern distortion, as illustrated in Fig. 2(d). These three types of feature distortion have been systematically investigated and presented below.

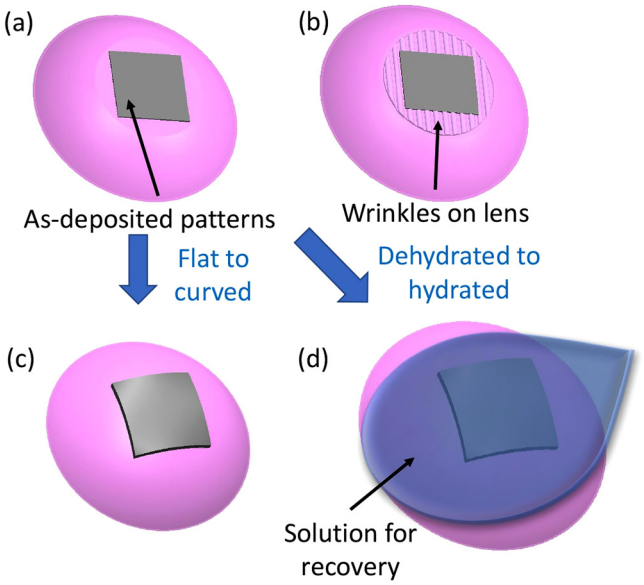

FIG. 2. Illustrations of (a) an as-deposited metallic pattern on a contact lens, and three types of pattern distortion on the contact lens, attributed to (b) wrinkles on the 3D-printed sample holder, (c) geometric transition of the lens from the flattened condition back to the original spherical shape, and (d) dehydration and hydration circles.

The surface smoothness of the 3D-printed sample holder is very important for the quality of the deposited metal features on contact lens. Figure 3(a) shows a sample holder printed by the conventional fused deposition modeling (FDM) method. The surface of such a holder typically has relief wrinkle features of 80 μm half pitch, which are formed due to the thermal stacking of filaments. Contact lenses are very sensitive to these surface features because of their flexibility and plasticity.[15–17] Figure 3(b) shows the photo of a contact lens dried on the FDM-printed holder, clearly bearing the surface wrinkles mechanically duplicated from the holder. Such linear wrinkles on the lens have an acute direction angle of θ in respective to the horizontal mask alignment marks, therefore shortening the edges of the metal square feature in the longitudinal direction. In addition, the height of the wrinkles leads to unwanted gaps between the contact lens and the shadow mask, further degrading the pattering fidelity of the deposited metal features. To address this issue, a stereolithography-based 3D printer is used to fabricate the sample holder with a much smoother surface and, subsequently, the contact lens dried on it also exhibits a smooth surface, as shown in Figs. 3(c) and 3(d), respectively. Figure 3(e) displays the optical microscope image of a typical Ti square pattern deposited on a contact lens dried on the SLA-printed sample holder. The orthogonal distortion of such a square pattern is quantitatively evaluated by the distortion ratio (DR) that is calculated by Eq. (1),

$$DR = \frac{W}{H} - 1, \tag{1}$$

where W and H are the edge lengths of the distorted square along transverse and longitudinal directions, respectively. 40 Ti square features are evaluated from a contact lens dried on the SLA-printed holder. For comparison, another 40 features fabricated on the FDM-printed holder are also evaluated. The statistical data are shown in Fig. 3(f). These data show that the samples from the FDM-printed holder generally have a DR of 5%, while the samples from the SLA-printed holder have a DR of less than 1%, indicating that the smoother surface of the holders results in less orthogonal distortion.

As mentioned above, when conformally flattened on the planar top surface of the sample holder, the central spherical cap region of the lens is inevitably deformed and compressed because of the nonzero Gaussian curvature of the spherical cap. Figure 4 shows the results of the FEA simulations performed by using Abaqus to quantitatively analyze the surface strain distribution over the flattened lens region. The central region for device fabrication has a relatively uniform strain around −3%.

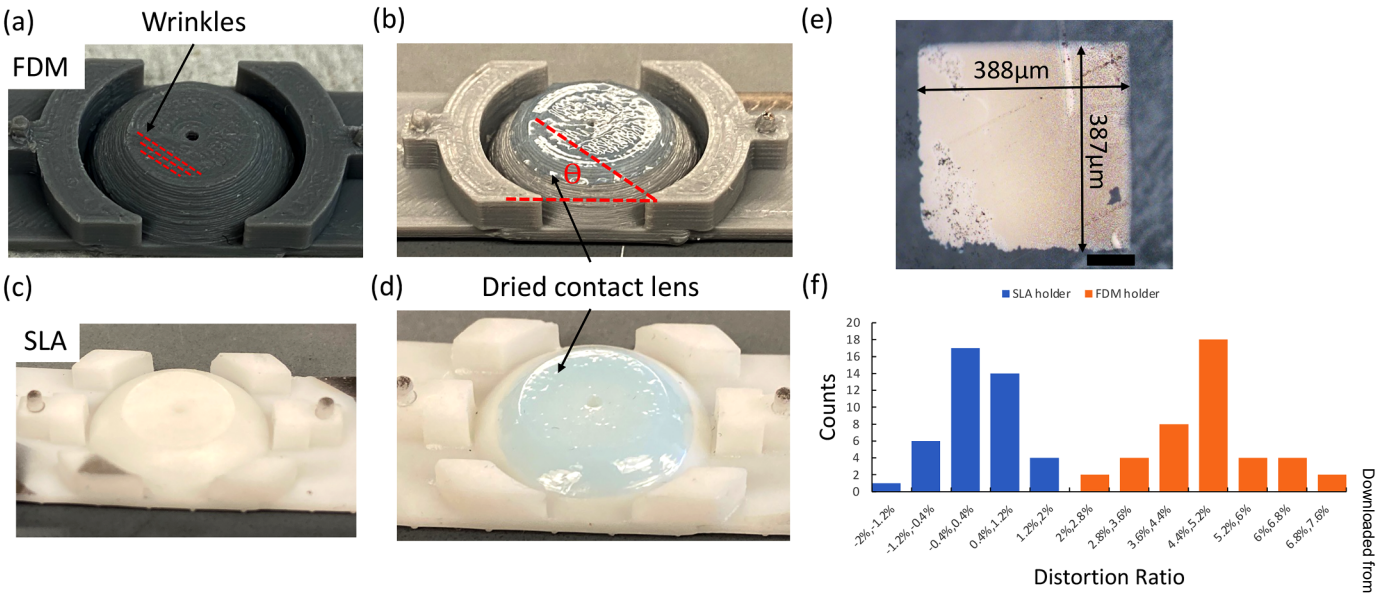

FIG. 3. Effects of the 3D printing methods on the SFD results: (a) and (b) display the photos of a sample holder 3D-printed by the FDM method resulting in wrinkles on the holder surface and a contact lens dried on it; (c) and (d) show the photos of a sample holder printed by the SLA method that results in a smooth holder surface and a contact lens dried on it; (e) optical microscope image of a Ti square feature deposited on the contact lens dried on the SLA-printed holder (scale bar:100 μm); (f) statistical distributions of the distortion ratio data collected from 40 square features deposited on the contact lenses dried on SLA-printed and FDM-printed holders.

Another important factor affecting the quality of the deposited Ti patterns is the volume change of the hydrogel material during a dehydration–rehydration circle. In this work, contact lenses are dehydrated in advance to enable the safe deposition of the metallic layer in the vacuum environment and rehydrated afterward for the implementation under the ambient condition. The overnight drying process can result in the evaporation of the solution in the hydrogel substrate, and the vacuum environment for the metal deposition does not cause a prominent morphological change in such a fully dehydrated substrate. Typically, 40–60 w/w% content of a contact lens is water, and it could shrink to less than half of its original volume after dehydration.[18–20] This huge volume change due to dehydration also implies that a comparable swelling is expected during the subsequent rehydration of the contact lens, which very likely causes pattern distortion and even cracks in the deposited metallic patterns. To suppress such pattern distortion or damage induced by dehydration, a mechanical load needs to be applied on the shadow mask during the dehydration process. Figure 5(a) shows the side-view photo of a contact lens drying under no load. Due to the shrinkage induced by dehydration, the skirt edge of the lens undergoes a relatively large displacement, as denoted by the dashed lines in Fig. 5(a). Figure 5(b) displays the counterpart result under a load, which exhibits a prominently reduced shrinkage due to dehydration. Figures 5(c) and 5(d) display the optical microscopic (OM) images of the deposited Ti ring patterns on two contact lenses rehydrated under no load and 0.02N load conditions, respectively. Under no load, the rehydration-induced free swelling of the hydrogel material leads to significant distortion of the Ti patterns, specifically widening the linewidth from 100 to 125 μm, and even generates cracks in the Ti features, as shown in Fig. 5(b). Such cracks further propagate to delaminate the metal layers from the lens substrate, leaving fragmentary patterns on the contact lens. Figure 5(d) implies that the dehydration–rehydration cycle under mechanical load results in prominently minimized lateral shrinkage of the lens film and, therefore, a more integral pattern with less distortion. Here, the linewidth only slightly increased by 5 μm.

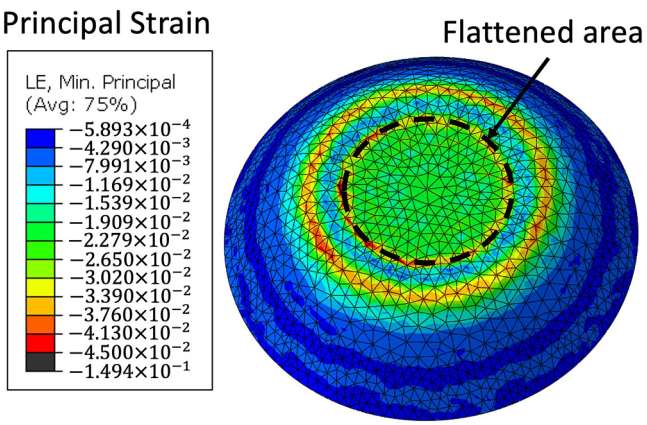

FIG. 4. FEA simulation result of the strain distribution over a contact lens (the flattened area is circled by the dark dashed line).

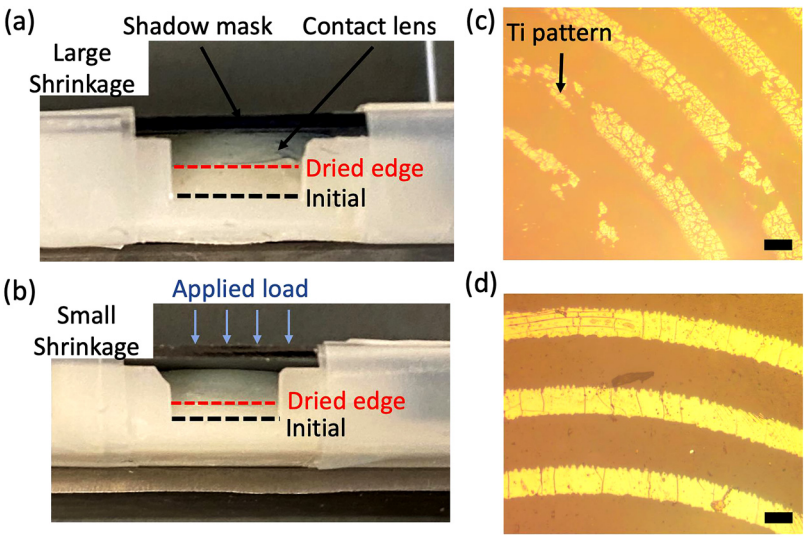

FIG. 5. Side-view photos of the shrunk contact lenses under (a) no applied load, (b) applied load. The final and initial skirt edge positions of the dried lens are marked by red and dark dashed lines, respectively. (c) and (d) are the optical images of the Ti ring patterns deposited on the rehydrated contact lenses corresponding to the drying conditions shown in (a) and (b), respectively (scale bar 100 μm).

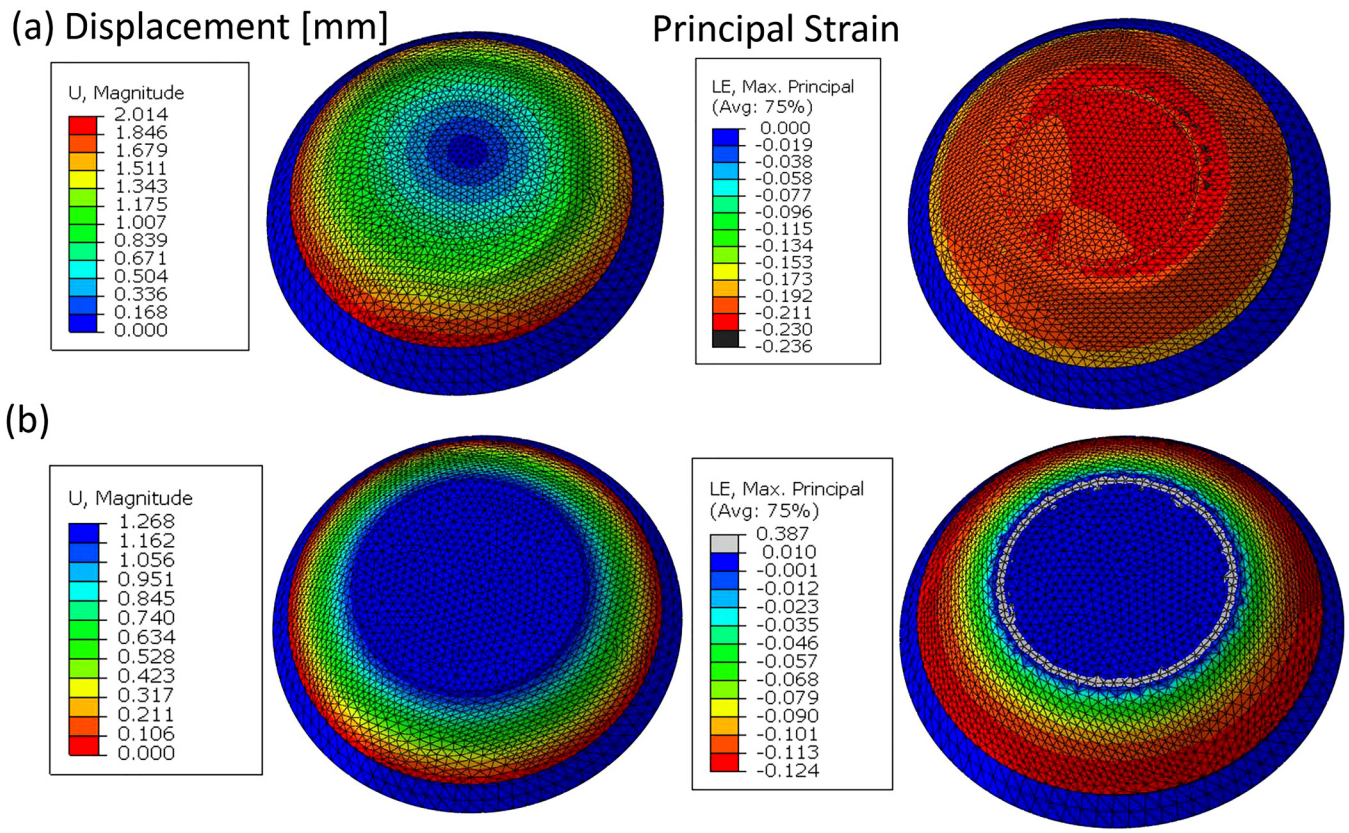

FIG. 6. Simulated displacement and surface strain distributions over a contact lens under (a) no applied pressure and (b) 1 mN pressure conditions.

TABLE I. FEA simulation results of the edge displacement and average planar strain within the flattened area of a contact lens under different pressure during the dehydration process.

Pressure (kPa)	Edge displacement (mm)	Ave. planar strain of flattened area
0	2.01	−23%
1.28	1.67	−10%
6.76	1.27	0
23.4	1.24	0
108	1.02	1%

To further analyze the effects of the applied loads on dehydration-induced shrinkage (or rehydration-induced swelling) of the hydrogel material as well as deposited metal patterns, a set of simulations have been performed using Abaqus. To provide a more generic and intuitive conclusion, the applied load is converted to the pressure value by dividing the load with the effective contact area between the hydrogel substrate and the shadow mask. Here, Young's modulus of wet contact lenses is 0.15 MPa, and the contact area between the contact lens and the shadow mask is 15.36 mm^2.[21] Figures 6(a) and 6(b) show the FEA simulation results of the displacement and principal strain of the contact lens due to the dehydration-induced shrinkage under no pressure and 6.76 kPa pressure conditions, respectively. Specifically, Fig. 6(a) shows that under no pressure condition, the skirt edge of the contact lens has a displacement of 2 mm and the average strain within the flattened central region is about −23%, which are consistent with the experimental observation in Fig. 5(a). Figure 6(b) indicates that under the pressure of 6.76 kPa, the central region of the lens exhibits negligible displacement or strain. In this case, the axial load exerted by the shadow mask is expected to induce lateral expansion of the hydrogel material and compensate the lateral shrinkage of the lens film due to dehydration. Table I lists the

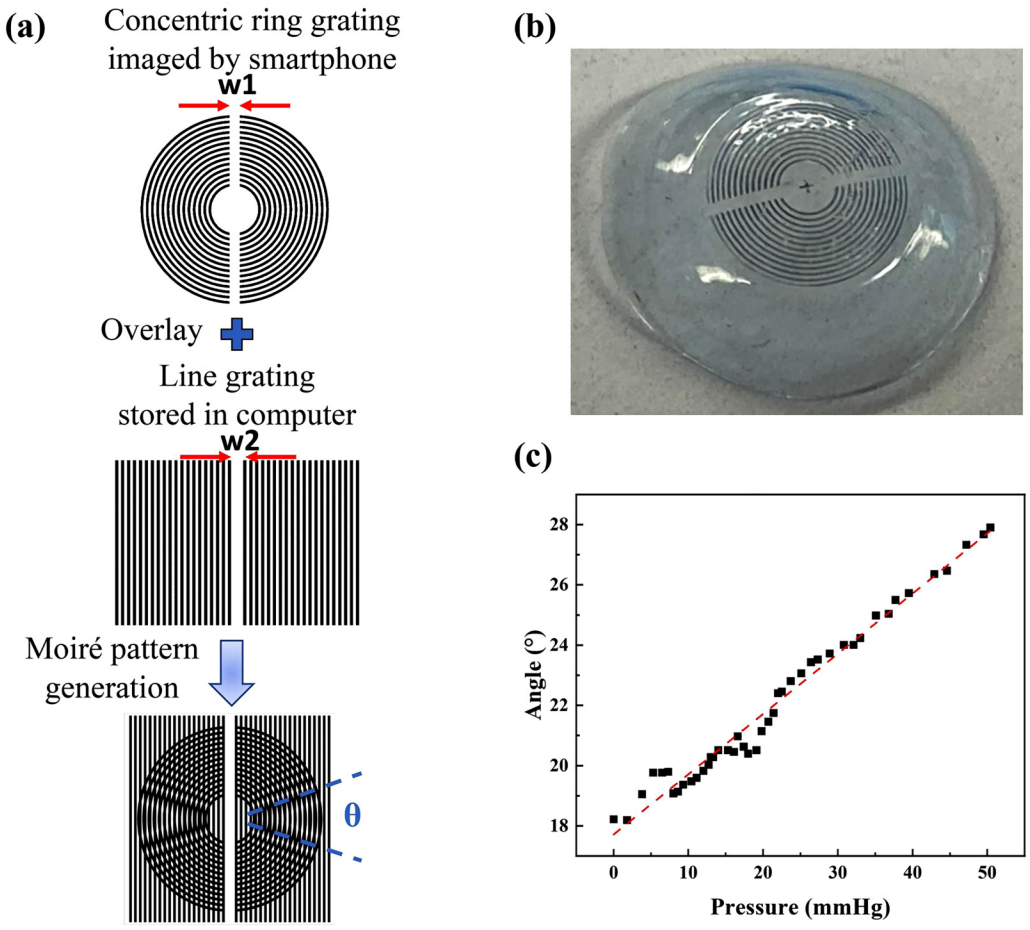

FIG. 7. (a) Operational principle of the contact lens IOP sensor; (b) a photo of a contact lens with a fabricated concentric ring grating. The pitch of the grating is 200 μm. W1 is 400 μm; (c) one representative IOP measurement. The pitch of the virtual line grating is 190 μm and W2 is 400 μm.

simulated data of edge displacement and average planar strain of the flattened area. Both parameters decrease as the applied load increases, and 6.76 kPa is estimated to be the threshold for effectively suppressing the lateral strain within the flattened area of the contact lens. Under the pressures over 108 kPa, the simulation is not convergent, implying the possible mechanical failure of the contact lenses under such high pressures.

Using the optimized fabrication process, a concentric ring grating (G1) is fabricated on the contact lens. As a result, a contact lens IOP sensor enabled by G1 on this contact lens and a virtual line grating (G2) stored in a computer can be achieved. The operational principle of this IOP sensor is illustrated in Fig. 7(a). Briefly, images of G1 are taken using a smartphone camera and subsequently transferred to a computer. Then moiré patterns are formed by superimposing images of G1 and G2 in a computer.[22] Finally, the central angle θ generated between two innermost adjacent moiré fringes is recognized as the IOP transducing signal. A photo of a contact lens with a concentric ring grating is shown in Fig. 7(b). One representative result of IOP measurements on a silicone eye model is shown in Fig. 7(c). It has been found that this IOP sensor can measure the IOP in a range of 0–50 mmHg with very good linearity and repeatability.

IV. SUMMARY AND CONCLUSION

In summary, we present shadow-mask-assisted flattening and deposition, a promising method capable of manufacturing reliable metallic patterns on curved and flexible hydrogel substrates. In this paper, the fabrication of microstructures on commercially available contact lenses is used as a technical demonstration. Specifically, in this process, the central region of a contact lens is conformally flattened on a sample holder and covered by a shadow-mask bearing predefined patterns, which serve as the windows for Ti layer deposition. This direct patterning method greatly reduces the fabrication cost of the metallic microstructures on curved and flexible hydrogel substrates. Using this method, we have demonstrated the production of Ti microstructures on the contact lens, one type of the most popular hydrogel-based device substrates and also experimentally and theoretically studied three key factors for obtaining a good yield and fidelity for the resultant Ti patterns on such hydrogel substrates, which include the surface smoothness of the 3D-printed sample holder, the shrinkage of the hydrogel material during dehydration–hydration cycles, and the geometric changes of the curved hydrogel substrates during the fabrication course. We also fabricated Ti-based concentric rings on the contact lenses and demonstrated that such function features can be used to measure the intraocular pressures on a silicone eye model, indicating its potential as a sensor for monitoring IOP *in vivo*. This process-oriented work provides a generic guideline for fabricating metallic microstructures on curved, flexible hydrogel substrates.

ACKNOWLEDGMENTS

This work was supported by the National Science Foundation (NSF) (No. CMMI-2001036). The authors would like to thank the staffs of the University of Michigan's Lurie Nanofabrication Facility for providing the support of device fabrication and Professor Long Que for the support of intraocular pressure data measurement. X.D. and L.Q. wish to thank the funds from the Exploratory Research Program (EPR) grant at Iowa State University.

AUTHOR DECLARATIONS

Conflict of Interest

The authors have no conflicts to disclose.

Author Contributions

M. Chen: Conceptualization (equal); Investigation (equal); Writing – original draft (equal); Writing – review & editing (equal). **X. Ding:** Conceptualization (equal); Investigation (equal); Writing – original draft (equal); Writing – review & editing (equal). **L. Que:** Supervision (equal). **X. Liang:** Supervision (equal).

DATA AVAILABILITY

The data that support the findings of this study are available from the corresponding author upon reasonable request.

REFERENCES

[1]A. Vásquez Quintero, R. Verplancke, H. De Smet, and J. Vanfleteren, Adv. Mater. Technol. **2**, 1700073 (2017).
[2]E. S. Izmailova *et al.*, Clin. Transl. Sci. **12**, 677 (2019).
[3]C. Choi *et al.*, Nat. Commun. **8**, 1 (2017).
[4]S.-K. Kim *et al.*, Adv. Mater. **34**, 2110536 (2022).
[5]R. Fu *et al.*, Chem. Mater. **31**, 9850 (2019).
[6]K. Pal, A. Banthia, and D. Majumdar, Afr. J. Biomed. Res. **9**, 23–29 (2006).
[7]A. Vasquez Quintero, R. Arai, Y. Yamazaki, T. Sato, and H. De Smet, Adv. Mater. Technol. **5**, 2000702 (2020).
[8]D. H. Keum *et al.*, Sci. Adv. **6**, eaba3252 (2020).
[9]J. Park *et al.*, Sci. Adv. **4**, eaap9841 (2018).
[10]J. Liu, S. Lin, X. Liu, Z. Qin, Y. Yang, J. Zang, and X. Zhao, Nat. Commun. **11**, 1 (2020).
[11]B. V. Muir, D. Myung, W. Knoll, and C. W. Frank, ACS Appl. Mater. Interfaces **6**, 958 (2014).
[12]M. A.-H. Gepreel and M. Niinomi, J. Mech. Behav. Biomed. Mater. **20**, 407 (2013).
[13]Y. L. Zhou, M. Niinomi, T. Akahori, H. Fukui, and H. Toda, Mater. Sci. Eng., A **398**, 28 (2005).
[14]G.-Z. Chen, I.-S. Chan, L. K. Leung, and D. C. Lam, Med. Eng. Phys. **36**, 1134 (2014).
[15]J. Wang, Z. Chen, X. Li, M. Liu, Y. Zhu, and L. Jiang, ACS Appl. Mater. Interfaces **11**, 41659 (2019).
[16]W. Wang, L. Xiang, D. Diaz-Dussan, J. Zhang, W. Yang, L. Gong, J. Chen, R. Narain, and H. Zeng, Chem. Mater. **32**, 10545 (2020).
[17]K. Peng, H. Yu, H. Yang, X. Hao, A. Yasin, and X. Zhang, Soft Matter **13**, 2135 (2017).
[18]M. Alam, M. A. Chowdhury, M. F. Hina, F. Akhtar, and S. Kabir, Chin. J. Polym. Sci. **22**, 253 (2004).
[19]E. M. Ahmed, J. Adv. Res. **6**, 105 (2015).
[20]S. Francis, D. Mitra, B. Dhanawade, L. Varshney, and S. Sabharwal, Radiat. Phys. Chem. **78**, 951 (2009).
[21]C. R. Horst, B. Brodland, L. W. Jones, and G. W. Brodland, Optometry Vision Sci. **89**, 1468 (2012).
[22]X. Ding and L. Que, "Design, modeling and validation of a flexible strain sensor based on moire patterns and image processing," in *2021 21st International Conference on Solid-State Sensors, Actuators and Microsystems (Transducers)* (IEEE, New York, 2021), pp. 1303–1306.